ISSN 0036-0244, Russian Journal of Physical Chemistry A, 2018, Vol. 92, No. 2, pp. 321–328. © Pleiades Publishing, Ltd., 2018.

STRUCTURE OF MATTER AND QUANTUM CHEMISTRY

Some Structural Properties of the Mixed Lead–Magnesium Hydroxyapatites[1]

K. Kaaroud[a], S. Ben Moussa[a], N. Brigui[a], and B. Badraoui[a,b,*]

[a] *U.R. Matériaux et synthèse organique UR17ES31, Institut Préparatoire aux Etudes d'Ingénieur de Monastir, Université de Monastir, Monastir, 5019 Tunisie*

[b] *U.R. Valorisation et Optimisation de l'Exploitation des Ressources, Université de Kairouan, Faculté des Sciences de sidi Bouzid 910*

**e-mail: badraoui_b@yahoo.fr*

Received October 11, 2016

Abstract—Lead–magnesium hydroxyapatite solid solutions $Pb_{(10-x)}Mg_x(PO_4)_6(OH)_2$ have been prepared via a hydrothermal process. They were characterized by X-ray powder diffraction, Transmission Electron Microscopy (TEM), chemical and IR spectroscopic analyses. The results of the structural refinement indicated that the limits of lead-magnesium solid solutions ($x \le 1.5$), a regular decrease of the lattice constant a and a preferential magnesium distribution in site S(I). Through the progressive replacement of Pb^{2+} ($r = 0.133$ nm) by the smaller cation Mg^{2+} ($r = 0.072$ nm), all interatomic distances decrease in accordance with the decrease of the cell parameters. According to what could be expected from the coordinance of the metallic sites S(I) (hexacoordination) and S(II) (heptacoordination), the small magnesium cation preferentially occupies the four sites S(I). The results of the TEM analysis confirm the presence of magnesium in the starting solution and reveals the decrease in the average size of crystals. The IR spectra show the presence of the absorption bands characteristic for the apatite structure.

Keywords: lead hydroxyapatite, Rietveld method, ionic substitution, IR spectroscopy

DOI: 10.1134/S0036024418020103

1. INTRODUCTION

The HAp crystallising in $P6_3/m$ are inorganic compounds allowing the incorporation of a wide range of different ionic substitutions [1–3]. The apatite structure can accommodate a great variety of other substituents and vacancies both in anionic and cationic sites. Divalent cations (Ca^{2+}, Sr^{2+}, Ba^{2+}, Mg^{2+}, Cd^{2+}, Pb^{2+}, ..., trivalent or tetravalent anions PO_4^{3-}, VO_4^{3-}, AsO_4^{3-}, SiO_4^{3-}, ..., and monovalent anions (OH^-, F^-, Cl^-, and Br^-) [4–7] have been reported to substitute into the HAp structure. The great variety of cationic and anionic substitutions is justified by the "open structure" of apatite. In the apatite structure, the cationic ions occupy two types of nonequivalent sites: in S(I), metallic ions are aligned in columns and surrounded by nine oxygen atoms at the fourfold symmetry 4*f* position, while in S(II) metallic ions are arranged in equilateral triangles centered on the screw axes, and are surrounded by seven oxygen atoms at the six-fold symmetry 6*h* position [1, 4]. Much limit of miscibility, morphology, stoichiometry and crystallinity levels can be obtained depending on the: (i) methods used for the synthesis process and (ii) the incorporation of foreign cations [8, 9]. In the available literature, only mixed lead hydroxyapatites are known for bicationic systems Pb–Ca, Pb–Cd, Pb–Sr, and Pb–Ba; they have been widely investigated [10–16]. For these systems, the limit of miscibility may be correlated to the relative properties of the metals (polarizability, electronegativity and essentially the cationic size). Structural refinements by Rietveld method of the mixed lead hydroxyapatite show that the smaller metal ions are distributed between the two crystallographic sites S(I) and S(II), with a strong preference to the smaller site S(I) [17–22]. The studies about the localization of cations in the apatite structure are even more interesting because the information acquired on the factors which drive the ion replacement can be extrapolated to the small substitutional range and hence to the field of the specific application [23–27]. A better understanding of the interaction of Mg with the lead hydroxyapatite structure could also provide useful information for clarifying the role of Mg in the formation of the hydroxyapatite solid solution. Herein, we report the results of a structural and spectroscopic investigation carried out on mixed Pb–Mg hydroxyapatites prepared by the hydrothermal synthesis from solutions

[1] The article is published in the original.

containing 0, 5, 7.5, 10, and 15 at % Mg. To simplify, the obtained hydroxyapatite solid solutions will be designated by the notation abbreviated Mg_xHAp (x is a number of magnesium atoms in the solid products).

2. EXPERIMENTAL PROCEDURE

2.1. Synthesis

The magnesium-substituted lead hydroxyapatite was synthesized by the hydrothermal method as follows [28, 29]. First, an aqueous solution (A) with concentration [P] = 0.25 mol L^{-1}, has been prepared by dissolving $(NH_4)_2HPO_4$ in distilled water. Next, a mixed aqueous solution (B), with a concentration [Pb] + [Mg] = 0.75 mol L^{-1} was prepared by dissolving lead and magnesium nitrates in distilled water. The 28 mL of (B) was added to the 50 mL of (A). The pH value of the solution is maintained approximately to 10 by a regular addition of small amounts of ammonia ($d = 0.89$; 28% aqueous solution). The obtained products were treated in autoclave under hydrothermal conditions at 120°C for 24 h. The products were filtered, washed with hot distilled water and dried at 100°C for 12 h. A thermal treatment at 400°C for 4 h was performed in order to improve its crystallinity. The reaction of the formation of the Mg-substituted lead hydroxyapatite is expressed as follows.

$$(10-x)Pb^{2+} + xMg^{2+} + 6PO_4^{3-} + 2OH^- \rightarrow Pb_{(10-x)}Mg_x(PO_4)_6(OH)_2; \quad x < 10.$$

All chemicals, $Pb(NO_3)_2$ (Prolabo, 99% purity), $Mg(NO_3)_2 \cdot 6H_2O$ (Labkem, 99% purity), and $(NH_4)_2HPO_4$ (Fluka, 98% purity), were of reagent grade and used without further purification.

2.2. Chemical Analyses and Instrumental Methods

The composition of the products was checked by the determination of Pb, Mg, and P contents. Magnesium and lead were determined by an atomic absorption spectrophotometry Perkin-Elmer 3110 spectrophotometer, and phosphorous was determined colorimetrically as phosphor-vanado-molybdate at 400 nm [30].

Powder X-ray diffraction (XRD) patterns were recorded using a PANalytical X'Pert PRO powder diffractometer equipped with a fast X'Celerator detector. Ni-filtered CuK_α radiation was used ($\lambda = 0.15418$ nm, 40 mA, 40 kV).

The broadening of the (002) and (310) reflections was used to assess the crystallite size $D_{(hkl)}$ along the c-axis and along a direction perpendicular to it. $D_{(hkl)}$ values were calculated from the widths at half maximum intensity ($\beta_{1/2}$) using the Scherrer equation [31] $D_{(hkl)} = \frac{K\lambda}{\beta_{1/2}\cos\theta}$, where λ is the wavelength, θ the diffraction angle, and K a constant depending on a crystal habit chosen as 0.9 for apatitic phases.

Fourier transform infrared spectroscopy (FTIR) analysis of the dry samples was done using FTIR spectrophotometer Nicolet 380 FTIR [32].

2.3. Structural Analysis

Rietveld refinement of the crystal structure of solid solutions was carried out using the Fullprof program [33]. The space group ($P6_3/m$) and the atomic positions of $Pb_{10}(PO_4)_6(OH)_2$ structure were utilized as starting data in the refinement [34]. No constraint was imposed on the overall magnesium content. Refinement of the occupancy factors was done only for Pb^{2+} and Mg^{2+} ions, with the assumption that these two cations were, initially, statistically located in the two cationic sites, (40% for the S(I) and 60% for the S(II)), the total contents answering to the stoichiometry obtained by chemical analysis. The occupancy factors of O and P were assumed constant, in agreement with the apatite stoichiometry. The fractional atomic coordinates were refined, starting from the atomic position of the two metals. No attempt was made to differentiate the magnesium positions from the lead ones [35]. Rietveld refinement was performed in several stages, the parameters obtained in each stage being deferred in the following. Then, the refined parameters are employed as an initial model for apatite with a magnesium content immediately greater, and so on.

3. RESULTS AND DISCUSSION

3.1. Chemical Analysis

The result of the chemical analysis reported in Table 1 is consistent with the formation of solid solutions of PbMgHAp. The values of Mg rise with the increase of Mg/(Pb + Mg) in the starting solution, in agreement with the quantitative incorporation of magnesium in the solid phase. The ratio between the two cations in the solid phase is very close to that in the synthesis solution, with the exception of

Table 1. The relative amount of magnesium in the solid products, evaluated through atomic absorption spectrometry reported as a function of strontium content in solution

Sample	Mg/(Pb + Mg) atomic ratio in solution	Mg/(Pb + Mg) atomic ratio in the solid product	(Pb + Mg)/P atomic ratio
PbHAp	0	0	1.665(5)
$Mg_{0.5}HAp$	0.50	0.52(5)	1.671(4)
$Mg_{0.75}HAp$	0.75	0.73(4)	1.663(3)
$Mg_{1.0}HAp$	1.00	0.98(3)	1.675(5)
$Mg_{1.5}HAp$	1.50	1.23(6)	1.663(3)

$Pb_{8.5}Mg_{1.5}HAp$, which exhibits an appreciably less magnesium incorporation. This suggests that the synthesized apatites are significantly stoichiometric, which indicates that the majority of the used magnesium has been incorporated in to solids. The atomic ratios (Pb + Mg)/P are close to the theoretical value of 1.667 for apatites.

3.2. X-ray Analysis

The results of the structural refinements indicate that the maximum amount of magnesium substitution in the lead hydroxyapatite PbHAp; accounts for about 15 at %. In other words, the upper limit of the solid solutions is $Pb_{8.5}Mg_{1.5}(PO_4)_6(OH)_2$. In spite of the limited range of magnesium incorporation, the decrease of the lattice parameter *a* and *c* in the apatitic structure. Although the difference in the cationic radii is small (Pb^{2+} coord. 7, radius 0.137 nm; Mg^{2+} coord. 7, radius 0.135 nm) [36], it should be the reason for the observed slight contraction of *a*- and *c*-axis. For high concentrations of magnesium (30% atom) in the starting solution, the X-ray diffraction pattern shows nonapatitic phases. Figure 1 displays the diagrams of diffraction X-rays of mixed hydroxyapatite samples. The unit cell dimensions, the agreement factors and the atomic positions are reported in Table 2.

The partial miscibility found for Pb–Mg apatites is in contrast with the behavior observed for Ca–Pb and Ca–Mg apatites. [37, 38] The partially miscibility of Ca and Mg hydroxyapatites is not surprising in view of their difference size, which is not the case for Ca and Pb ions. The miscibility of the Ca–Pb hydroxyapatites can be justified on the basis of the large difference in the polarizabilities of calcium and lead ions: Ca^{2+} is a hard acid, giving mainly ionic interactions with oxygen, whereas Pb^{2+} is a soft acid, displaying a considerable tendency towards polarization and covalent interactions. In the Pb–Mg case, we have two hard acids. Their significant tendency towards covalent interactions and directional bonding, which is most likely the origin of the large distortions of the (PO_4) tetrahedra, probably limits the possibility of mutual substitution. In particular, the precipitation of nonapatitic phases at high magnesium concentrations suggests that the presence of lead, even in small amounts, inhibits the formation of MgHA. It has been reported that it is quite difficult for divalent cations with an ionic radius smaller than that of Ca^{2+}, such as Zn^{2+}, Ni^{2+}, Co^{2+}, Mn^{2+}, and Cu^{2+}, to substitute for Ca^{2+} in the apatite structure, and are known to inhibit the synthesis of hydroxyapatite [39–43]. Examination of Table 2 shows that the position of the (OH) ion shifts progressively along the *c*-axis direction. In the apatitic channel of lead apatite, the (OH) ions are positioned very close to the mid-point between the planes of the S(II) triangles. As the content Mg increases, the hydroxide ions move regularly towards the center of S(II) triangles. A similar phenomenon was observed for the displacement of the (OH^-) ion in the calcium–lead and cadmium–lead hydroxyapatite series [18, 35]. The substitution of calcium or cadmium for lead causes a shift of the OH group position towards the center of S(II) triangles. In those cases, the driving force was ascribed to the ionic radii difference. Indeed, when the site S(II) is mainly occupied by Pb atoms, the space at the center of S(II) triangles is reduced significantly and the hydroxyl ion must be accommodated outside. In the present case, the effect is even more evident, because a large difference in the ionic size of Pb^{2+} and Mg^{2+} radii $r(Pb^{2+}) - r(Mg^{2+}) = 0.061$ nm.

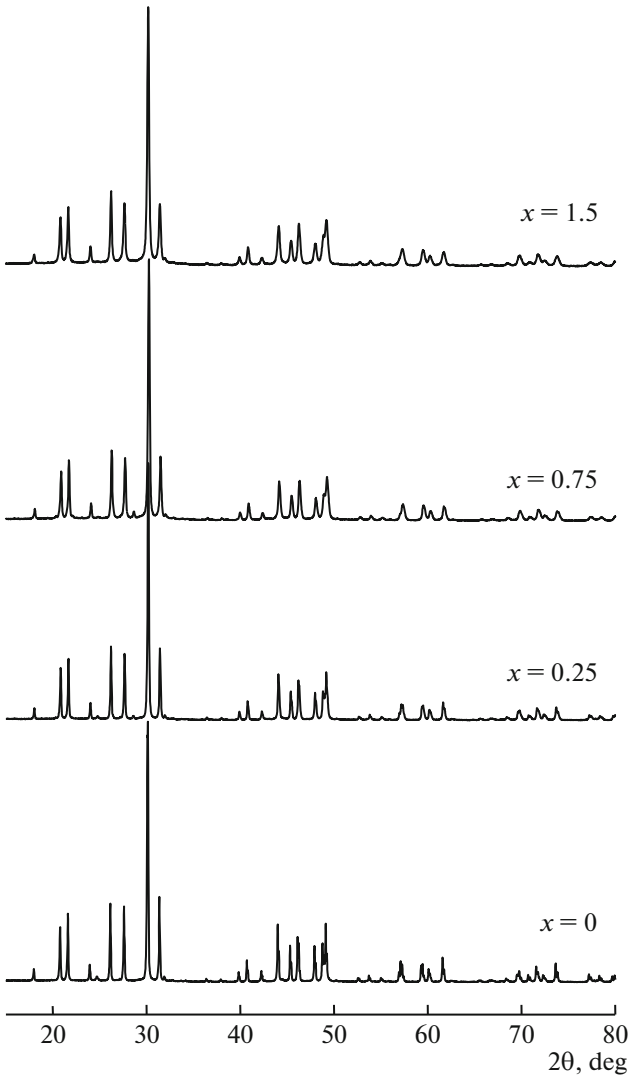

Fig. 1. Powder X-ray diffraction patterns of the samples (PbHAp), $Mg_{0.5}Hap$, $Mg_{0.75}HAp$, $Mg_{1.0}HAp$, and $Mg_{1.5}HAp$.

The results of the powder fitting structure refinements indicate a clear preference of magnesium for site S(I) of the apatite structure. This result is clearly shown in Table 3. Furthermore, this is in agreement

Table 2. Fractional atomic coordinates and equivalent thermal parameters, after Rietveld refinement, for the mixed Pb–Mg hydroxyapatites (e.s.d. in parentheses)

$Pb_{(10-x)}Mg_xHAp$	Atom	x	y	z	B, Å^2
PbHAp	$a = 0.9880(5)$	$c = 0.7402(2)$	$Rp = 7.21$	$Rwp = 7.76$	$\chi^2 = 3.12$
	{Pb(1)}	0.3333	0.6667	−0.0061(8)	0.632
	{Pb(2)}	0.2477(7)	0.0010(5)	0.2500	0.840
	P	0.394(6)	0.365(4)	0.2500	1.056
	O(1)	0.329 (5)	0.475(5)	0.2500	1.482
	O(2)	0.571(5)	0.458(7)	0.2500	1.504
	O(3)	0.338(6)	0.263(5)	0.084(1)	1.385
	O(H)	0.000	0.0000	0.040(6)	1.220
$Mg_{0.5}HAp$	$a = 0.9859(3)$	$c = 0.7357(4)$	$Rp = 8.25$	$Rwp = 8.12$	$\chi^2 = 3.04$
	{Pb(1), Mg(1)}	0.3333	0.6666	0.0010(5)	0.293
	{Pb(2), Mg(2)}	0.2495(2)	1.0036(6)	0.2500	0.799
	P	0.393(3)	0.354(3)	0.2500	0.187
	O(1)	0.345(5)	0.495(5)	0.2500	0.483
	O(2)	0.566(5)	0.485(4)	0.2500	0.311
	O(3)	0.322(1)	0.248(2)	0.083(2)	0.154
	O(H)	0.000	0.000	0.082(3)	0.701
$Mg_{0.75}HAp$	$a = 0.9807(2)$	$c = 0.7322(5)$	$Rp = 9.04$	Rwp=9.46	$\chi^2 = 2.84$
	{Pb(1), Mg(1)}	0.3333	0.6666	0.0022(6)	0.299
	{Pb(2), Mg(2)}	0.2496(2)	1.0025(4)	0.2500	0.612
	P	0.398(2)	0.364(2)	0.2500	0.940
	O(1)	0.348(5)	0.484(2)	0.2500	0.782
	O(2)	0.576(1)	0.472(4)	0.2500	1.405
	O(3)	0.327(4)	0.253(4)	0.086(3)	0.611
	O(H)	0.000	0.000	0.122(4)	0.390
$Mg_{1.0}HAp$	$a = 0.9762(3)$	$c = 0.7261(5)$	$Rp = 9.02$	$Rwp = 8.55$	$\chi^2 = 2.82$
	{Pb(1), Mg(1)}	0.3333	0.6666	0.0044(5)	0.223
	{Pb(2), Mg(2)}	0.2482(2)	0.9991(7)	0.2500	0.601
	P	0.409(4)	0.382(4)	0.2500	0.988
	O(1)	0.347(5)	0.503(5)	0.2500	0.492
	O(2)	0.594(2)	0.455(2)	0.2500	0.995
	O(3)	0.355(3)	0.286(3)	0.085(3)	0.418
	O(H)	0.000	0.000	0.166(7)	1.241
$Mg_{1.5}HAp$	$a = 0.9732(4)$	$c = 0.7165(6)$	$Rp = 10.13$	$Rwp = 9.04$	$\chi^2 = 2.73$
	{Pb(1), Mg(1)}	0.3333	0.6666	0.0107(5)	0.599
	{Pb(2), Mg(2)}	0.2515(4)	1.0015(7)	0.2500	0.702
	P	0.414(3)	0.391(4)	0.2500	0.416
	O(1)	0.334(2)	0.487(5)	0.2500	0.504
	O(2)	0.611(5)	0.475(3)	0.2500	0.730
	O(3)	0.348(2)	0.284(2)	0.094(4)	1.304
	O(H)	0.000	0.000	0.162(3)	1.395

Table 3. Statistic distribution and refinement occupancy of magnesium atoms in the two metal sites S(I) and S(II) of Pb–Mg hydroxyapatites

Sample	Chemical analysis	Refinement analysis	Refinement distribution (A)		Statistic distribution (B)		$(A - A/B)$	
			S(I)	S(II)	S(I)	S(II)	S(I)	S(II)
$Mg_{0.5}HAp$	0.52	0.495	0.291	0.204	0.204	0.309	+0.426	–0.339
$Mg_{0.75}HAp$	0.73	0.744	0.432	0.312	0.297	0.446	+0.454	–0.300
$Mg_{1.0}HAp$	0.98	0.995	0.625	0.370	0.398	0.597	+0.570	–0.380
$Mg_{1.5}HAp$	1.23	1.206	0.774	0.432	0.482	0.723	+0.605	–0.402

with the preference of Pb for site S(II), where the arrangement of the "staggered" equilateral triangles allows for the optimization of the packing of larger ions, in contrast to site S(I) where the strict alignment of the columns causes a stronger repulsion. However, the refinement shows that the occupancy factor of magnesium in the S(I) site is always higher than that corresponding to the statistical distribution (Fig. 2). For the sample $Pb_{8.5}Mg_{1.5}(PO_4)_6(OH)_2$, the discrepancy between the value of the magnesium content obtained from the Rietveld refinement and the value measured by chemical analysis, can be ascribed to the greatest amount of magnesium must be on the crystal surface and/or in the amorphous phase and may reflect the smaller ionic radius of Mg^{2+} (0.72 Å) than in Pb^{2+} (1.33 Å) and the difference in the polarizability and electronegativity of Mg^{2+} and Pb^{2+} cations. In agreement with bibliographic revues, the same observation has been reported for Mg and Zn substituted calcium hydroxyapatite [44, 45].

In Table 4 the P–O, M–O, and M–M interatomic distances are reported. The values of the mean M(I)–O and M(II)–O distances slightly decrease when the amount of magnesium in the hydroxyapatite increases (in agreement with the reduction of the a-axis).

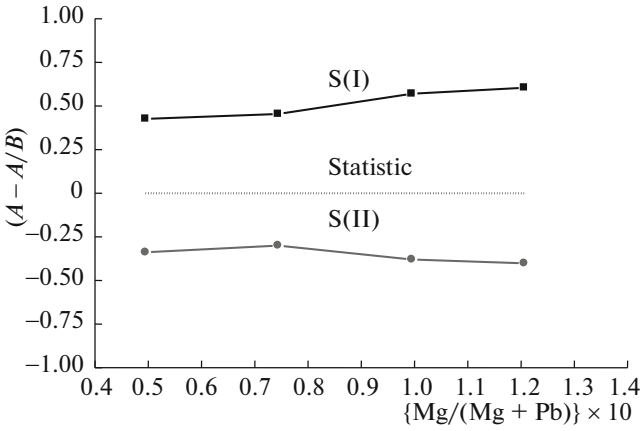

Fig. 2. Relative difference distribution of magnesium atoms between S(I) and S(II) crystallographic sites. The lines are to guide the eyes.

The line profile analysis has been applied in order to investigate the line broadening increase and the peak shifts observed in the XRD patterns of the samples. A qualitative estimation of the crystal size as derived from the Scherrer equation, (Table 5). $D_{(002)}$ is related to the mean crystallite size along the c-axis, whereas $D_{(310)}$ refers to the mean crystal size along a direction perpendicular to it. The variation of the $D_{(hkl)}$ values as a function of the magnesium atomic percentage present in the solid phase indicate that the dimensions of the apatitic crystallites are strongly affected by the presence of even a very small amount of magnesium in the solid phase.

3.3. Infrared Absorption Spectroscopy

The infrared spectra of the mixed hydroxyapatites present the characteristic absorption bands (stretching and bending) of the PO_4^{3-} group and OH^- ions of the apatitic structure, two of them are reported in Fig. 3. The

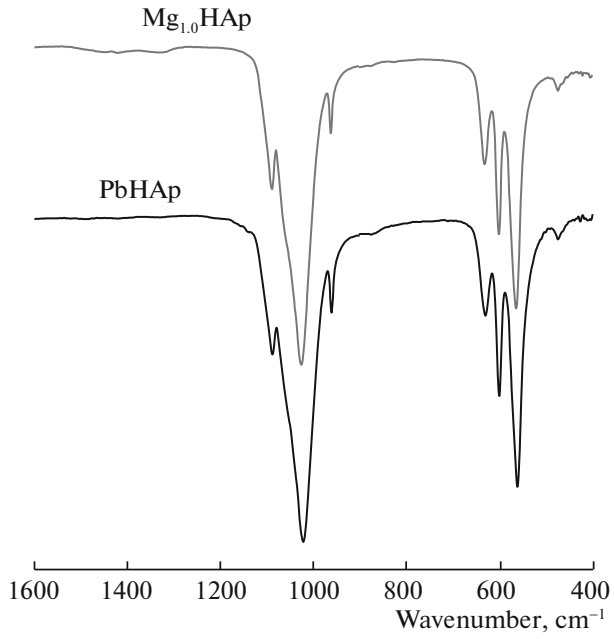

Fig. 3. Infrared spectra of PbHAP and $Mg_{1.0}HAp$.

Table 4. M–O, M–OH, and M–M distances (nm) in mixed Pb–Mg hydroxyapatites (e.s.d. in parentheses)

	PbHAp	$Mg_{0.5}$HAp	$Mg_{0.75}$HAp	$Mg_{1.0}$HAp	$Mg_{1.5}$HAp
M(I)–O(1)	0.2665(1)	0.2570(3)	0.2613(3)	0.2554(1)	0.2491(2)
M(I)–O(2)	0.2534(2)	0.2792(3)	0.2722(5)	0.2513(1)	0.2505(4)
M(I)–O(3)	0.2982(4)	0.3145(2)	0.3041(4)	0.2891(4)	0.2913(2)
⟨M(I)–O⟩	**0.2727**	**0.2835**	**0.2792**	**0.2652**	**0.2636**
M(II)–O(1)	0.2912(2)	0.3005(1)	0.3107(3)	0.3055(4)	0.2956(3)
M(II)–O(2)	0.2562(3)	0.2382(3)	0.2443(1)	0.2522(3)	0.2425(2)
M(II)–O(3)	0.2553(1)	0.2515(3)	0.2492(2)	0.2586(2)	0.2591(3)
M(II)–O(3)	0.2582(6)	0.2492(2)	0.2614(1)	0.2603(2)	0.2652(5)
M(II)–OH	02927(2)	0.2825(2)	0.2796(2)	0.2654(2)	0.2492(2)
⟨M(II)–O⟩	**0.2644**	**0.2581**	**0.2628**	**0.2644**	**0.2621**
M(II)–M(II)	0.4244(2)	0.4502(4)	0.4471(4)	0.4327(2)	0.4304(6)
M(I)–M(II)	0.4215(4)	0.4249(5)	0.4173(2)	0.4104(5)	0.4027(4)
M(I)–M(I)	0.3593(2)	0.3645(5)	0.3692(3)	0.3522(5)	0.3452(6)

Table 5. Crystallite size $D_{(002)}$ and $D_{(310)}$ of the Mg-substituted lead hydroxyapatites in the direction normal to (002) and to (310) planes

Sample	$\beta_{1/2}$ (002) (rad) × 10^{-4}	$D_{(002)}$ (nm)	$\beta_{1/2}$ (310) (rad) × 10^{-4}	$D_{(310)}$ (nm)
PbHAp	17.453	81.2	19.373	76.3
$Mg_{0,5}$HAp	18.151	78.1	19.547	75.7
$Mg_{0.75}$HAp	19.373	73.2	22.165	66.8
$Mg_{1.0}$HAp	20.594	68.8	24.085	61.4
$Mg_{1.5}$HAp	25.132	56.4	24.434	60.5

absence of the bands due to CO_3^{2-} and HPO_4^{2-} ions indicates the absence of appreciable amount of impurities [46, 47]. The progressive substitution of the lead ions for magnesium induces a regular shift of the absorption bands towards smaller wavenumbers. Furthermore, the infrared spectra of some mixed hydroxyapatites does not show the band of the symmetric deformation of ions the PO_4^{3-}, not the band reflecting the movement of libration of (OH^-) ions. These two bands may be masked by the band of skew-symmetric deformation of ions PO_4^{3-} [48]. The shift of the absorption bands of the PO_4 group can be attributed to the variation of the nature of the metal-oxygen interactions [49]. The character of lead-oxygen interaction is more covalent than that of magnesium-oxygen and furthermore a cation of larger mass is involved. The more covalent character of the Pb–OH leads to a shift of the OH vibrational modes towards a lower frequency.

3.4. TEM Observations

Transmission electron microscopy (TEM) micrographs analysis of the samples are illustrated in Fig. 4. From the photomicrographs, it can be seen that the size of precipitated apatite particles. PbHAp is constituted of plate-shaped crystals. After the substitution of

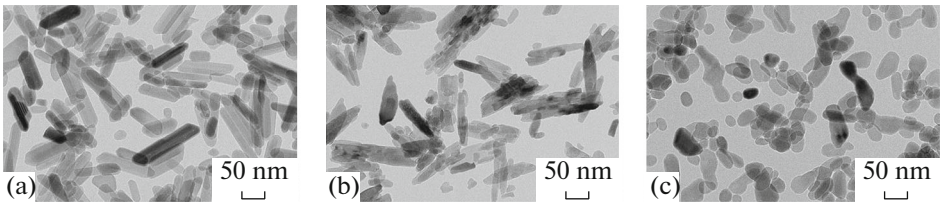

Fig. 4. TEM images of PbHAp (a), $Mg_{0.75}$Hap (b), and $Mg_{1.5}$Hap (c).

magnesium, their shapes transformed into tiny crystals with rod-like morphology. Moreover, the presence magnesium at the start solution reveals the decrease of the average size of these crystals with a strong tendency to aggregate. The results of the TEM analysis agree well with the analysis of XRD pattern.

CONCLUSION

Lead-magnesium hydroxyapatite solid solutions $Pb_{(10-x)}Mg_x(PO_4)_6(OH)_2$ were prepared by a hydrothermal process. The results of this study indicate that the great difference between cationic radii of Pb^{2+} and Mg^{2+} ions allows the formation of the limited lead-magnesium solid solutions ($x \leq 1.5$). The progressive incorporation of the Mg^{2+} cation in the lead hydroxyapatite induces a contraction of the *a* lattice constant. Structural refinements by Rietveld method show that the Mg^{2+} ions are distributed between the two crystallographic sites S(I) and S(II), with a low preference to the smaller site S(I). This is particularly marked for low Mg^{2+} concentrations. The magnesium exhibits an evident inhibiting role on the synthesis of mixed lead-magnesium hydroxyapatite through a reduction of the crystallite sizes.

ACKNOWLEDGMENTS

We are thankful to the INRAP (Institut National de Recherche and d'Analyses Physico-chimiques), the RTCEn (Research and Technology Centre for Energy) and the University of Monastir (Tunisia). We are also very grateful to Mr. Ali Hadroug for his valuable help with English.

REFERENCES

1. D. Laurencin, N. Almora-Barrios, N. H Leeuw, C. Gervais, C. Bonhomme, F. Mauri, W. Chrzanowski, J. C. Knowles, R. J. Newport, A. Wong, Z. Gan, and M. E. Smith, Biomaterials **32**, 1826 (2011).
2. K. Pardun, L. Treccani, E. Volkmann, P. Streckbein, C. Heiss, J. W. Gerlach, S. Maendl, and K. Rezwan, J. Biomater. Appl. **30**, 104 (2015).
3. E. Bertoni, A. Bigi, G. Cojazzi, M. Gandol, S. Panzavolta, and N. Roveri, J. Inorg. Biochem. **72**, 29 (1998).
4. J. C. Elliott, *Structure and Chemistry of the Apatites and Other Calcium Orthophosphates* (Elsevier, Amsterdam, 1994).
5. D. McConnel, *Apatites, Applied Mineralogy* (Springer, New York, Vienna, 1963).
6. N. V. Bulina, M. V. Chaikina, I. Y. Prosanov, D. V. Dudina, and L. A. Solovyov, J. Solid State Chem. **252**, 93 (2017).
7. R. Z. LeGeros, M. H. Taheri, G. B. Quirolgico, and J. P. Legeros, in *Proceedings of the 2nd International Conference on Phosphorus Compounds, 1980,* p. 89.
8. I. Khattech and M. Jemal, Thermochim. Acta Crystallogr. B **45**, 247 (1989).
9. A. Nounah and J. L. Lacout, J. Solid State Chem. **107**, 444 (1993).
10. I. Ntahomvukiye, I. Khattech, and M. Jemal, Ann. Chim. **22**, 435 (1997).
11. A. Bigi, A. Ripamonti, S. Brückner, M. Gazzano, N. Roveri, and S. A. Thomas, Acta B **45**, 247 (1989).
12. A. Bigi, E. Boanini, C. Capuccini, and M. Gazzano, Inorg. Chim. Acta **360**, 1009 (2007).
13. A. Bigi, M. Gazzano, A. Ripamonti, E. Foresti, and N. Roveri, J. Chem. Soc., Dalton Trans., 241 (1986).
14. A. A. Hamad, B. Badraoui, and M. Debbabi, J. Soc. Chim. Tunis. **5**, 115 (2003).
15. A. A. Hamad, B. Badraoui, and M. Debbabi, J. Soc. Alger. Chim. **13**, 131 (2003).
16. I. Khattech and M. Jemal, Thermochim. Acta **298**, 23 (1997).
17. B. Badraoui, A. Bigi, M. Debbabi, M. Gazzano, N. Roveri, and R. Thouvenot, Eur. J. Inorg. Chem. **7**, 1864 (2002).
18. B. Badraoui, A. Aissa, A. Bigi, M. Debbabi, and M. Gazzano, Mater. Res. Bull. **44**, 522 (2009).
19. B. Badraoui, R. Thouvenot, and M. Debbabi, C.R. Acad. Sci. Paris, Ser. 2c: Chim. **3**, 107 (2000).
20. A. Aissa, B. Badraoui, R. Thouvenot, and M. Debbabi, Eur. J. Inorg. Chem. **19**, 3828 (2004).
21. B. Badraoui, A. Aissa, and M. Debbabi, J. Phys. Chem. Solids **68**, 211 (2007).
22. B. Badraoui, A. Aissa, A. Bigi, and M. Gazzano, J. Solid State Chem. **179**, 3065 (2006).
23. J. Batton, A. J. Kadaksham, A. Nzihou, and N. Aubry, J. Hazard. Mater. **139**, 461 (2007).
24. Z. Boukha, M. Kacimi, M. F. R. Pereira, J. L. Faria, J. L. Figueiredo, and M. Ziyad, Appl. Catal. A **317**, 299 (2007).
25. R. Jagannathan and T. R. N. Kutty, J. Lumin. **71**, 115 (1997).
26. E. Kendrick, M. S. Islam, and P. R. Slater, J. Mater. Chem. **17**, 3104 (2007).
27. S.V. Dorozhkin, Mater. Sci. **42**, 1061 (2007).
28. Demazeau, C.R. Acad. Sci. Paris, Ser. 2c, No. 2, 685 (1999).
29. R. E. Riman, W. L. Suchanek, and M. M. Lencka, Ann. Chim. Sci. Mater. **15**, 27 (2002).
30. A. Gee and U. R. Deitz, Anal Chem. **25**, 1320 (1953).
31. H. P. Klug and L. E. Alexander, *X-ray Diffraction Procedures for Polycrystalline and Amorphous Materials* (Wiley, New York, 1969).
32. R. N. Hannah and J. S. Swinehart, *Experiments in Technique of Infrared Spectroscopy* (Perkin-Elmer, Norwalk, CN, 1974).
33. J. Rodriguez-Carvajal, Physica B **192**, 55 (1993).
34. S. Brückner, G. Lusvardi, L. Menabue, and M. Saladini, Inorg. Chim. Acta **236**, 209 (1995).
35. B. Badraoui, A. Bigi, M. Debbabi, M. Gazzano, N. Roveri, and R. Thouvenot, Eur. J. Inorg. Chem. **5**, 1261 (2001).
36. R. D. Shannon, Acta Crystallogr. A **32**, 751 (1976).
37. A. Bigi, M. Gazzano, A. Ripamonti, E. Foresti, and N. Roveri, J. Chem. Soc., Dalton Trans., 241 (1986).

38. T. Turki, A. Aissa, H. Agougui, and M. Debbabi, J. Soc. Chim. Tunis. **12**, 161 (2010).

39. N. sendi, H. Bachouâ, B. Badraou, and E. Elaloui, Ann. Chim. Sci. Mater. **38**, 95 (2013).

40. A. Bigi, A. Ripamonti, A. Bruckner, S. Gazzano, M. Roveri, and N. Thomas, Acta Crystallogr. B **45**, 247 (1989).

41. B. Badraou, H. Bachouâ, and M. Othmani, Ann. Chim. Sci. Mater. **33**, 329 (2008).

42. M. Othmani, A. Aissa, and H. Bachouâ, Appl. Surf. Sci. **264**, 886 (2013).

43. A. Farzadi, F. Bakhshi, M. Solati-Hashjin, M. Asadi-Eydivand, and N. Azuan abu Osman, Ceram. Int. **40**, 6021 (2014).

44. A. Bigi, G. Falini, E. Foresti, M. Gazzano, A. Ripaonti, and N. Roveri, J. Inorg. Biochem. **49**, 69 (1993).

45. T. Turki, M. Othmani, C. Goze Bac, F. Rachdi, and K. Bouzouita, Appl. Surf. Sci. **284**, 66 (2013).

46. G. Engel and W. E. Klee, J. Solid State Chem. **5**, 28 (1972).

47. B. O. Fowler, Inorg. Chem. **13**, 207 (1974).

48. M. Andres-Verges, F. J. Higes-Rolando, C. Valenzeula-Calahorro, and P. F. Gonzalez-Diaz, Spectrochim. A **39**, 1077 (1983).

49. C. E. Weir and E. R. Lippincot, J. Res. Natl. Bureau Stand. A **65**, 173 (1961).